Cement and Concrete Research 39 (2009) 126–139

Contents lists available at ScienceDirect

Cement and Concrete Research

journal homepage: http://ees.elsevier.com/CEMCON/default.asp

Improvement of the chloride ingress resistance of OPC mortars by using spent cracking catalyst

E. Zornoza [a], P. Garcés [b], J. Payá [a], M.A. Climent [b,*]

[a] Dept. Ingeniería de la Construcción, Universidad Politécnica de Valencia, Spain
[b] Dept. Ingeniería de la Construcción, Universidad de Alicante, Spain

ARTICLE INFO

Article history:
Received 22 March 2007
Accepted 25 November 2008

Keywords:
Transport properties
Chloride
Pozzolan
Mortar
Corrosion

ABSTRACT

The influence of the incorporation of spent cracking catalyst (FC3R) on the chloride ingress resistance has been evaluated. Thermogravimetric analyses have shown that the pozzolanic reaction of FC3R yields higher contents of hydrated calcium aluminates and silicoaluminates, so chloride binding capacity of mortars was highly improved. Mercury intrusion porosimetry analyses demonstrated that FC3R produces a significant reduction of capillary pore volume. As a result non-steady-state and steady-state chloride diffusion coefficients were reduced, enhancing the chloride ingress resistance of mortars incorporating FC3R. Additionally, the corrosion behaviour of steel embedded in Portland cement mortars partially substituted by spent cracking catalyst (FC3R) under chloride attack has been studied. Results showed that the incorporation of FC3R decreased the corrosion rates of steels and increased chloride thresholds for corrosion. For this reason, FC3R is an interesting pozzolanic material that can be used in reinforced concrete for civil engineering applications exposed to the action of chlorides.

1. Introduction

Corrosion of reinforcing steel is of great concern because it is probably the most widespread cause of degradation of reinforced concrete. Initially, reinforcing steel embedded in concrete is naturally protected from corrosion by the high alkalinity of its pore solution [1]. However, this passive state can be broken by the destruction of the passive film that protects steel reinforcement. The main agents leading to destruction of the passive film are penetration of chlorides and carbon dioxide.

Steel reinforced concrete can be exposed to the action of chlorides during its service life, for example, in marine structures, in which reinforced concrete is partially submerged in seawater, which has very high concentration of chloride. Another typical situation is the use of de-icing salts (normally NaCl) in roads and bridges located in cold climate regions. These situations can notably reduce the service life of a structure and also can increase the maintenance and repair costs of affected elements.

Once the reinforced concrete is in contact with chlorides, they penetrate into the concrete cover at a rate that will depend on the external chloride concentration, the porosity of concrete, the chloride binding capacity of the cementitious matrix and some environmental parameters such as the relative humidity and temperature. When a sufficient amount of chlorides reaches the surface of steel reinforcements, a local breakdown of the passive layer takes place, and then, reinforcements start to corrode. For this reason, it is a matter of interest to increase the time that chlorides need to penetrate the concrete cover. In the effort of finding new mix designs that can improve the chloride ingress resistance of the concrete cover, researchers usually try to decrease the porosity and to enhance the chloride binding capacity of the cementitious matrix. One of the parameters that are important in the study of the chloride-induced corrosion of steel reinforcement is the chloride threshold. This threshold is usually defined as the amount of chlorides expressed as a percentage respect to cement mass needed to start the corrosion of steels embedded in the cementing matrix. A widely used value is 0.4% Cl^- respect to cement mass.

Zeolitic catalysts are widely used in petrochemical refining (400,000 tons/year). When the catalytic properties of this product are degraded, the deactivated catalyst must be replaced. The chemical composition of spent cracking catalyst (FC3R), silicoaluminates with a zeolitic structure, allows it to be used in concrete, due to its high pozzolanic activity [2–10]. These species, containing high amounts of Al_2O_3, form during hydration calcium aluminate and calcium silicoaluminate compounds, which can bind chlorides coming from external sources, thereby reducing the potential for corrosion of reinforcements. The formation of Friedel's salt acts as a barrier to the chloride ingress through the cementitious matrix and delays the reaching of chlorides to the reinforcing steel, so its formation is beneficial because increases the initiation period of the chloride-

* Corresponding author.
E-mail address: ma.climent@ua.es (M.A. Climent).

0008-8846/$ – see front matter © 2008 Elsevier Ltd. All rights reserved.
doi:10.1016/j.cemconres.2008.11.006

induced corrosion process of reinforcing steel. Therefore, FC3R can affect two factors in the transport of chloride through concrete: the porosity of the cementitious paste is potentially reduced, due to the pozzolanic reaction; and also chloride binding capacity is improved.

The aim of this work is to evaluate the behaviour of Portland cement-FC3R mortars in a chloride-contaminated environment. Chloride migration tests were used to determine the chloride ingress resistance of mortars. Also corrosion rate of reinforcing steels embedded in these mortars were monitored when exposed to an external source of chlorides and carbonation. An additional study was made to approximate the chloride threshold by means of including different levels of chlorides in the mixing water of the mortars.

2. Experimental

2.1. Migration tests specimens and procedure

Cylindrical mortar specimens (diameter 10 cm, height 12 cm) were prepared using cement type CEM I 52.5 R, normalized siliceous sand, distilled water and spent cracking catalyst (FC3R). Table 1 summarizes chemical composition of cement and FC3R. FC3R was previously ground to activate its pozzolanic activity in a laboratory ball-mill for 20 min [2,7,11]. Several water/binder ratios (w/b=0.3, 0.4, 0.5 and 0.7) and cement substitutions by FC3R (0, 5, 10, 15 and 20%) were used. A polycarboxilic superplasticizer (Sika Viscocrete) was used in mortars with low w/b ratio (0.3 and 0.4) to maintain the workability in minimum acceptable values. This workability was determined through the flow table spread test (FTS) [12], being the minimum value for this property 13.5 cm. A constant sand/binder ratio of 3/1 was used. Mix proportions of the mortars prepared are presented in Table 2.

After their preparation, specimens were submerged in water for curing during 28 days. Then, two discs (diameter 10 cm, thickness 15 mm) were extracted from each specimen. These discs were the samples to be tested in the chloride migration tests, so the values presented in this work are the mean value of these two replicates of each specimen. Prior to the performance of the test, the samples were water saturated in order to eliminate the air of the pores. The water saturation procedure was the following [13]: samples were introduced in a desiccator with a vacuum pump connected for 3 h; then, the desiccator was filled with water with the vacuum pump connected for 1 h; finally, the vacuum pump was switched off and the samples remained in the desiccator for 18 h.

Fig. 1 shows a scheme of the migration cell used in the migration tests, whose design has been previously used by other authors [14,15]. The mortar sample was placed in the migration cell separating the cell in two chambers. One of the chambers (anodic chamber) was filled with de-ionized water, the other one (cathodic chamber) was filled with a solution of NaCl 1 M. Two graphite electrodes were placed in each chamber and a DC potential of 12 V was applied between them. With this arrangement, chlorides are forced to migrate through the mortar sample, from the cathodic chamber to the anodic one.

Table 1
Chemical composition of cement and FC3R used

Parameter	Cement (%)	FC3R (%)
LOI	2.34	1.50
SiO_2	20.21	48.2
Al_2O_3	4.94	46.0
Fe_2O_3	2.85	0.95
CaO	62.87	–
MgO	1.05	–
Na_2O	0.10	0.50
K_2O	0.95	–
SO_3	3.37	0.04

Table 2
Mix proportions used in the preparation of the migration test specimens

Specimen (w/b–% FC3R–% Plast)	Cement (g)	FC3R (g)	Water (g)	Sand (g)	Plasticizer (g)
0.3–0–1	450	0	135	1350	4.5
0.3–5–1.5	427.5	22.5	135	1350	6.75
0.3–10–2	405	45	135	1350	9
0.3–15–2.5	382.5	67.5	135	1350	11.25
0.3–20–3	360	90	135	1350	13.5
0.4–0–0.5	450	0	180	1350	2.25
0.4–5–0.5	427.5	22.5	180	1350	2.25
0.4–10–0.5	405	45	180	1350	2.25
0.4–15–1	382.5	67.5	180	1350	4.5
0.4–20–1	360	90	180	1350	4.5
0.5–0–0	450	0	225	1350	0
0.5–5–0	427.5	22.5	225	1350	0
0.5–10–0	405	45	225	1350	0
0.5–15–0	382.5	67.5	225	1350	0
0.5–20–0	360	90	225	1350	0
0.7–0–0	450	0	315	1350	0
0.7–5–0	427.5	22.5	315	1350	0
0.7–10–0	405	45	315	1350	0
0.7–15–0	382.5	67.5	315	1350	0
0.7–20–0	360	90	315	1350	0

During the migration test, the conductivity of the anodic chamber was monitored, as well as the effective potential difference between both sides of the sample and the temperature. Conductivity values (C) were transformed in chloride concentration by means of Eq. (1), which was previously reported [15], and concentration values were plotted versus time. From this graph two parameters are obtained: the chloride flux (from the slope), and the time lag needed for chlorides to appear in the anodic chamber.

$$[Cl^-]\,(\mathrm{mM}) = -1.71 + 11.45 \times C\,(\mathrm{mS/cm}) \quad (1)$$

From the values of the chloride flux and the time lag it is possible to derive both the steady-state (D_s) and the non-steady-state (D_{ns}) chloride diffusion coefficients [15]. These coefficients are expressed in m^2/s. Steady and non-steady state diffusion coefficients were calculated from plots of conductivity versus time through the following equations:

$$D_s = \frac{Jx}{\upsilon C_1 \gamma} \quad (2)$$

$$D_{ns} = \frac{2x^2}{\tau \upsilon^2}\left[\upsilon \coth\frac{\upsilon}{2} - 2\right] \quad (3)$$

where J is the chloride flux, x is the specimen thickness, C_1 is the chloride concentration in the catholyte, γ is the activity coefficient of

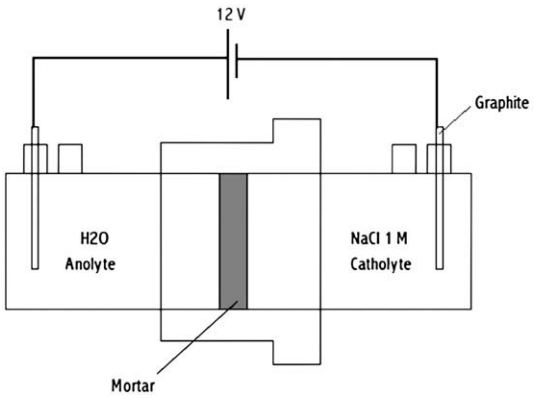

Fig. 1. Scheme of the migration cell used in the chloride migration tests.

chlorides in the catholyte, τ is the time lag for the chloride appearance in the anolyte and υ is:

$$\upsilon = \frac{zF\Delta\Phi}{RT} \quad (4)$$

where z is charge of chlorides, F is the Faraday's constant and $\Delta\Phi$ is the voltage drop between both sides of the mortar, R is the gas constant and T is the temperature. The resistivity of mortars used in migration tests was measured, after the water saturation step but before the migration test. For this purpose, corrosion rate measurement equipment (model Gecor 8 from Geocisa, Spain) was used.

2.2. Mercury intrusion porosimetry

The pore structure of some selected samples of the mortars prepared for migration tests was analyzed by mercury intrusion porosimetry: w/b ratio of 0.5, 0% and 15% of FC3R, before and after the performance of the migration test. Three samples (1 cm^3) of each selected mortar were analyzed. A mercury intrusion porosimeter model Autopore IV 9500 V1.05 from Micromeritics Instrument Corporation was used for the analysis. The pressure range of this equipment is 0.003 to 227.5 MPa.

2.3. Thermogravimetric and XRD analyses

Cement pastes with different levels of substitution (0, 5, 10, 15, 20%) of cement by FC3R were prepared. Constant w/b ratio of 0.5 was used in the preparation of the pastes. Pastes were mixed in 100 ml plastic containers and were cured for 28 days covered with a thin film of de-ionized water to avoid excessive leaching from the paste. Then, pastes were submerged in 1 M NaCl solution for 6 months. Finally, pastes were placed in a carbonation chamber (100% CO_2, 65 ± 5% RH) for 1 month. Samples of the pastes were extracted from the outer part of each paste at the following times: (1) after the curing, (2) after 1 month, (3) 2 months, (4) 6 months submerged in the NaCl solution and (5) after 6 months submerged in the NaCl solution followed by 1 month in the carbonation chamber.

The sample consisted of a little portion of the paste that was ground. Non-combined water of the paste was removed by successive washings with acetone and filtration. Then samples were dried in a furnace at 60 °C for 20 min. Finally, samples were sieved with an 80-μm sieve. The fraction that passed the sieve was the sample to be analyzed by thermogravimetry (about 30 mg). The analyses were performed in a thermogravimetric scale Mettler Toledo TGA850. Samples were subjected to a heating ramp of 10 °C/min from 35 °C to 600 °C using a sealed aluminium crucible with a pinhole. The test atmosphere was nitrogen, fed at a rate of 75 ml/min.

XRD analysis were made of samples with a 15% of cement replacement by FC3R. These samples were prepared following the same protocol than that explained for thermogravimetric analysis after the 28-day curing period and after 15-day period of immersion in NaCl solution. Analyses were made with a PW1710 diffractometer. Diffraction angles (2θ) were those obtained by using $K_{\alpha 1}$ of a copper cathode (0.154056 nm). Scanning was made in the 4°–60° angle range.

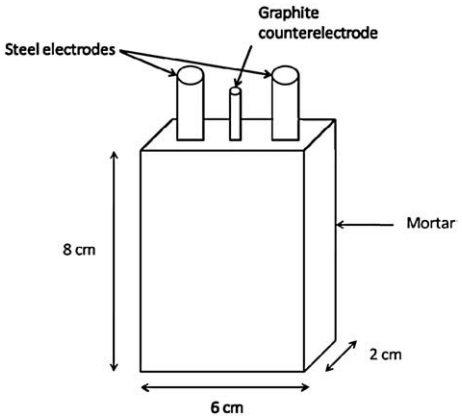

Fig. 2. Scheme of the corrosion rate specimen.

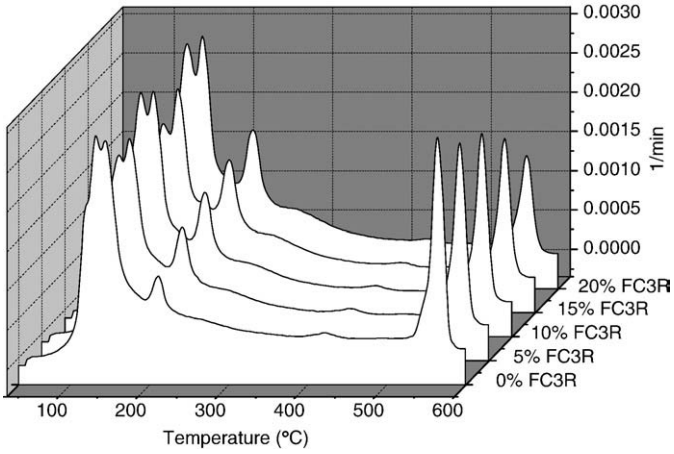

Fig. 3. DTG curves of cement pastes with different levels of FC3R substitution after curing for 28 days.

2.4. Corrosion rate specimens and procedure

Some selected mix proportions of those presented in Table 2 were used for the preparation of corrosion rate specimens (mortars with w/b ratio of 0.5 and 0.7). Fig. 2 shows the prismatic mortar specimens used in this study. Two steel electrodes (10 mm diameter) and one graphite counter-electrode were embedded in the specimens. The resulting thickness of the mortar cover for the electrodes was 5 mm. During the duration of the tests, specimens were subjected successively to different environments: in 100% of relative humidity (RH) for 100 days; partially submerged in a 0.5 M NaCl solution for 125 days; again in 100% RH for 40 days; in a carbonation chamber (100% CO_2, 65 ± 5% RH to obtain a rapid carbonation of samples [16,17]) for 100 days; and finally, in a 80% RH for 80 days.

Another set of specimens were used for the study of the chloride content threshold needed for depassivating the steels embedded in the cement matrices. For this part of the research only mortars with w/b ratio of 0.5 and 15% cement substitution by FC3R were prepared, as well as the corresponding control mortars without FC3R. These specimens were prepared adding NaCl to the mixing water to obtain different proportions of chlorides in each mortar: 0, 0.5, 1, 2 and 5% of chlorides by cement mass. These specimens were stored in a humid chamber with 85% of RH.

After the specimen preparation, corrosion rate (Icorr) and corrosion potential (Ecorr) were monitored periodically until the end of the test. All corrosion potentials are referred to a saturated calomel electrode (SCE). Corrosion rate measurements were made by the polarization resistance technique [18] using a scanning potentiostat model EG&G 362 from Princeton Applied Research. The potential scan

Table 3
Thermogravimetric mass losses of cement pastes with different levels of FC3R substitution after curing for 28 days

FC3R (%)	Fixed lime (%)	Mass loss (%)			
		Total	$Ca(OH)_2$	C–S–H	CAH–CASH
0	0	20.59	3.11	17.12	0.36
5	12.68	20.17	2.58	16.99	0.61
10	19.19	21.22	2.26	18.21	0.75
15	27.79	19.9	1.91	17.17	0.82
20	43.45	21.28	1.41	18.95	0.92

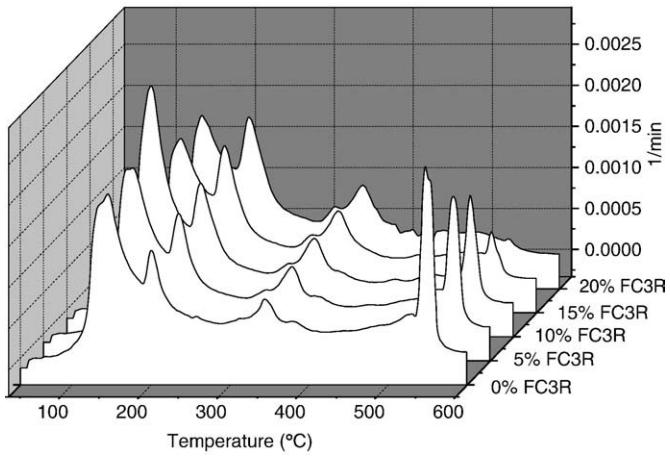

Fig. 4. DTG curves of cement pastes with different levels of FC3R substitution after 6 months of immersion in NaCl 1 M.

was made between −10 mV and +10 mV respect to the corrosion potential of each steel electrode. The scanning rate was 0.5 mV/s. Ecorr and Icorr values presented in this work are the mean values of two electrodes embedded in each specimen.

After the corrosion tests were performed, mortar specimens were broken and the steel electrodes were extracted. These electrodes were cleaned and weighted to compare the electrochemical mass loss (calculated by integrating the Icorr vs time graph and applying Faraday's law) with the gravimetric mass loss (obtained by the difference between initial and final mass of steel electrodes).

3. Results and discussion

3.1. Thermogravimetric analyses

Fig. 3 shows the derivative curve of the thermograms (DTG) of the samples with different level of cement substitution by FC3R after 28 days of curing. Three main peaks can be observed: first, in the 100–180 °C range, the dehydration of hydrated calcium silicates (C–S–H) and ettringite; second, at about 200 °C, the dehydration of hydrated calcium aluminates (CAH) and aluminosilicates (CASH); and third, at 550 °C, the decomposition of portlandite (CH) [7,11,19,20]. Little qualitative differences can be observed in the DTG curves. Table 3 presents thermogravimetric mass losses of these pastes. For increasing amounts of FC3R, a decrease in the portlandite content can be observed as a consequence of the pozzolanic reaction and the lower cement content. Additionally, the formation of CASH and CAH is enhanced by the presence of FC3R because these phases are the principal products of the pozzolanic reaction of FC3R.

Fig. 4 shows DTG curves of the samples with different level of cement substitution by FC3R after immersion in NaCl 1 M solution for 6 months. In this case, apart from the peaks previously mentioned, a new one can be observed at 350 °C. This mass loss belongs to the decomposition of Friedel's salt ($Ca_2Al(OH)_6Cl{\cdot}2H_2O$) [21]. The presence of Friedel's salt was confirmed by XRD analysis as shown in Fig. 5. As it was expected, Friedel's salt was formed after the immersion in NaCl solution as a result of the reaction between CAH and chlorides through the following mechanism that implies two steps:

$$Ca(OH)_2 + 2NaCl \rightarrow 2NaOH + CaCl_2 \quad (5)$$

$$CaCl_2 + Ca_3Al_2O_6{\cdot}8H_2O + 2H_2O \rightarrow Ca_4Al_2O_6Cl_2{\cdot}10H_2O \quad (6)$$

It can be appreciated in Eq. (5) that the formation of Friedel's salt also consumes some of the alkaline reserve [22–24]. Table 4 shows thermogravimetric mass losses of cement pastes with different levels of FC3R substitution after 6 months of immersion in NaCl 1 M. In this table it can be observed that the amount of portlandite has decreased with respect to samples after 28 days of curing, due to the formation of Friedel's salt Eq. (5). This reduction cannot be attributed only to the evolution of the pozzolanic reaction because FC3R mainly reacts in the first weeks of curing [7,11] and the portlandite content of sample without FC3R has also decreased. Additionally, the Friedel's salt content increases with the cement substitution level, so it is clear the

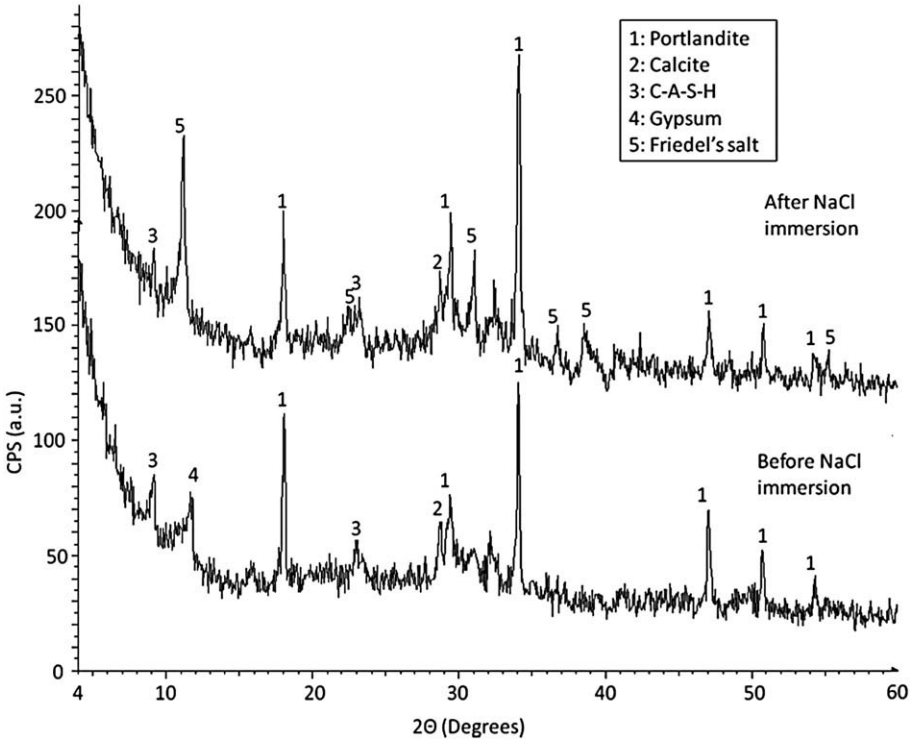

Fig. 5. XRD analyses of cement pastes with 15% of FC3R before and after immersion in 1 M NaCl solution during 15 days.

Table 4
Thermogravimetric mass losses of cement pastes with different levels of FC3R substitution after 6 months of immersion in NaCl 1 M

FC3R (%)	Mass loss (%)		
	$Ca(OH)_2$	Friedel's salt	CAH–CASH
0	2.13	0.31	0.44
5	1.37	0.42	0.64
10	1.09	0.50	0.81
15	0.35	0.54	0.93
20	0	0.55	1.10

effect of FC3R on the chloride binding capacity of cementitious matrices. The higher formation of CAH and CASH of FC3R-containing pastes offers an improvement in the chloride ingress resistance of such cementitious matrices.

Fig. 6 shows DTG curves of cement pastes with different levels of FC3R substitution after the accelerated carbonation process. It can be observed that both peaks of portlandite and Friedel's salt have disappeared as a consequence of the carbonation. Portlandite reacts with CO_2 to yield calcium carbonate, which decomposes at more than 700 °C and is not shown in this figure. The decomposition of Friedel's salt in presence of CO_2 is a consequence of the reduction of the pH (equivalent to the reduction of OH^- concentration) in the pore solution that carbonation produces, and it is explained by the mechanism shown in Eq. (7) [25–27]. Then the release of chlorides bound to the cementitious matrix takes place. This phenomenon is a major risk for reinforcing steel corrosion because two factors converge: the reduction of the alkalinity of the pore solution and the increase of free chlorides content.

$$Ca_4Al_2O_6Cl_2 \cdot 10H_2O \leftrightarrow 4Ca^{2+} + 2Cl^- + 6OH^- + 2Al(OH)_3 + 4H_2O \qquad (7)$$

The quantification of portlandite content in all the samples studied is presented in Fig. 7. As it was previously mentioned, the increase in the FC3R content produces a decrease of the portlandite of pastes. Furthermore, the formation of Friedel's salt also produces an additional decrease in portlandite. This can be observed in the decrease produced between samples taken after 28 days of curing and those taken after immersion in NaCl for one month. Additionally, the formation of Friedel's salt takes place very fast because no further decrease in the portlandite content is observed after the first month of immersion. Finally, as expected, after the carbonation process, there is no portlandite remaining in the pastes.

The quantification of Friedel's salt content in all the samples studied is presented in Fig. 8. In this figure it is clearly observed that the formation of Friedel's salt is produced during the first month of immersion in the NaCl solution. It can be also noted that the increasing amount of FC3R produces an increase in the formation of Friedel's salt. Finally, the accelerated carbonation process reverses the formation of Friedel's salt as was commented.

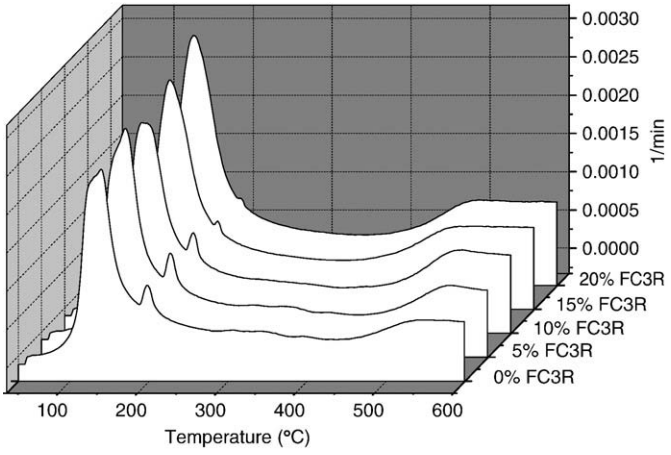

Fig. 6. DTG curves of cement pastes with different levels of FC3R substitution after carbonation.

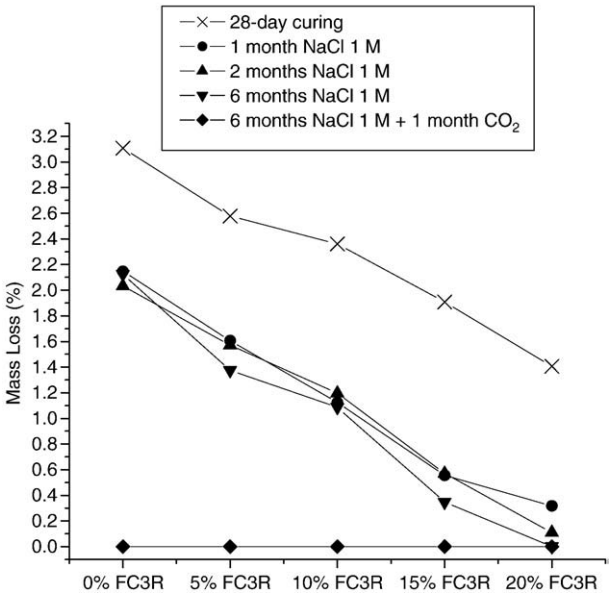

Fig. 7. Quantification of portlandite dehydration in the samples through the overall process.

In Fig. 9, the quantification of the dehydration of CAH–CASH phases is presented. When the FC3R substitution is increased, a higher formation of CAH–CASH is observed. Thus, the chloride binding potential of the samples is enhanced. Data plotted in Fig. 9 also supports the fact that the pozzolanic reaction of FC3R is fast, because after curing, there is only a minor increase in CAH–CASH content. Finally, as was pointed out in other works [16,27], the carbonation also affects CAH–CASH. Calcium from these compounds reacts with CO_2 when portlandite is exhausted, to produce calcium carbonate and aluminium hydroxide.

3.2. Chloride migration tests

Fig. 10 shows the evolution of the chloride concentration for migration tests performed on mortar specimens with all the w/b

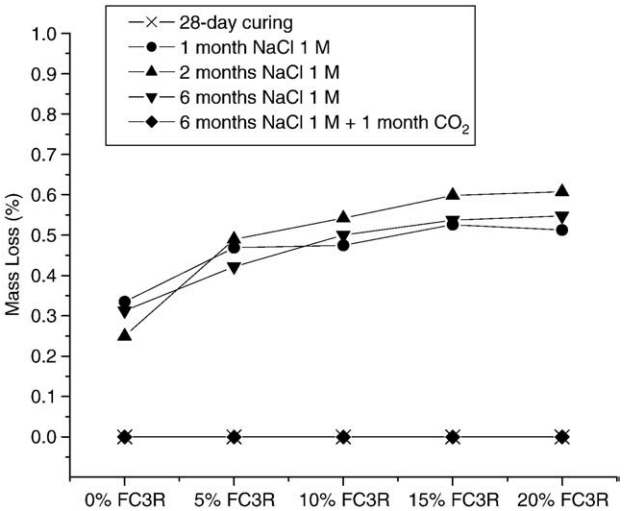

Fig. 8. Quantification of Friedel's salt decomposition in the samples through the overall process.

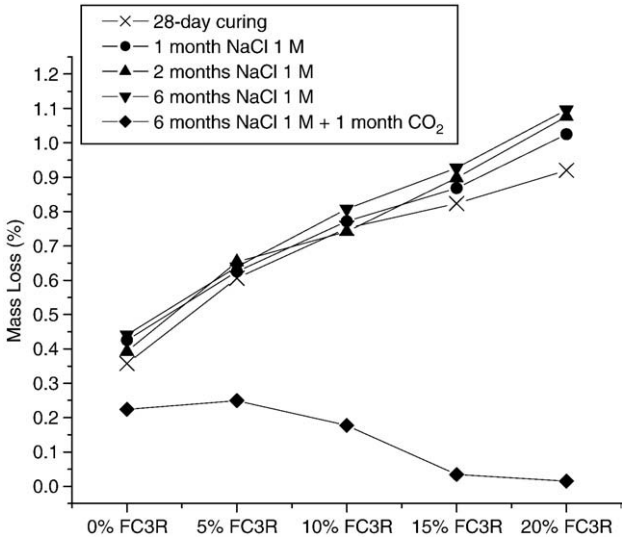

Fig. 9. Quantification of CAH–CASH dehydrations in the samples through the overall process.

ratios and 0% and 15% of cement substitution by FC3R. In this figure it can be observed that mortars with 15% of FC3R offer lower slopes, so the chloride flux through the samples is higher for mortars without FC3R for any w/b ratio. It can be also appreciated that the total chloride amount at the end of the migration test is lower for mortars with higher w/b ratio. This phenomenon is produced because the effective potential difference between both sides of the mortar is higher when the w/b ratio is increased because the electrical conductivity of the mortar is higher. It should be noted that the effective potential difference plus the voltage drop due to the ohmic resistance of the mortar is the voltage applied to the electrodes (12 V). Therefore, the potential difference at the interface between electrode and solution in the anolyte chamber is higher for mortars with high w/b ratio, and the chloride oxidation at the anode takes place at lower chloride concentrations than those observed for the mortars with low w/b ratio. This fact does not affect the test because the parameter of interest is the slope of the graph.

Additionally, the time lag is higher for mortars with 15% of FC3R, except for w/b of 0.3. The monitoring parameters and the results of the migration tests are shown in Table 5.

In Fig. 11, it is presented the influence of the substitution level of FC3R on the evolution of the chloride concentration in the anodic chamber for the w/b of 0.5. Table 5 shows the slopes and the time lags corresponding to these specimens. It can be observed that when the cement substitution is increased, the slope decreases and the time lag increases.

A similar behaviour can be observed for mortars prepared with a w/b ratio 0.3. Fig. 12 shows the migration results obtained for mortars with different FC3R substitution and w/b ratio of 0.3, and Table 5 presents the parameters obtained from this set of mortars. It is again noticeable that the increase in the substitution level produces a decrease of the chloride flux through the mortar and a delay in the time lag, except for mortar with 20% of FC3R. This exception comes from the fact that FC3R is a high water-demanding pozzolan. With such a low w/b ratio and high proportion of FC3R, the workability of the mortar is significantly reduced, even though the high dosage of superplasticizer. Therefore, these mortars showed some difficulty for compaction.

Figs. 13 and 14 show non-steady-state (D_{ns}) and steady-state (D_s) chloride diffusion coefficients obtained for all the mortars studied, respectively. Both figures show clearly the significant reduction of

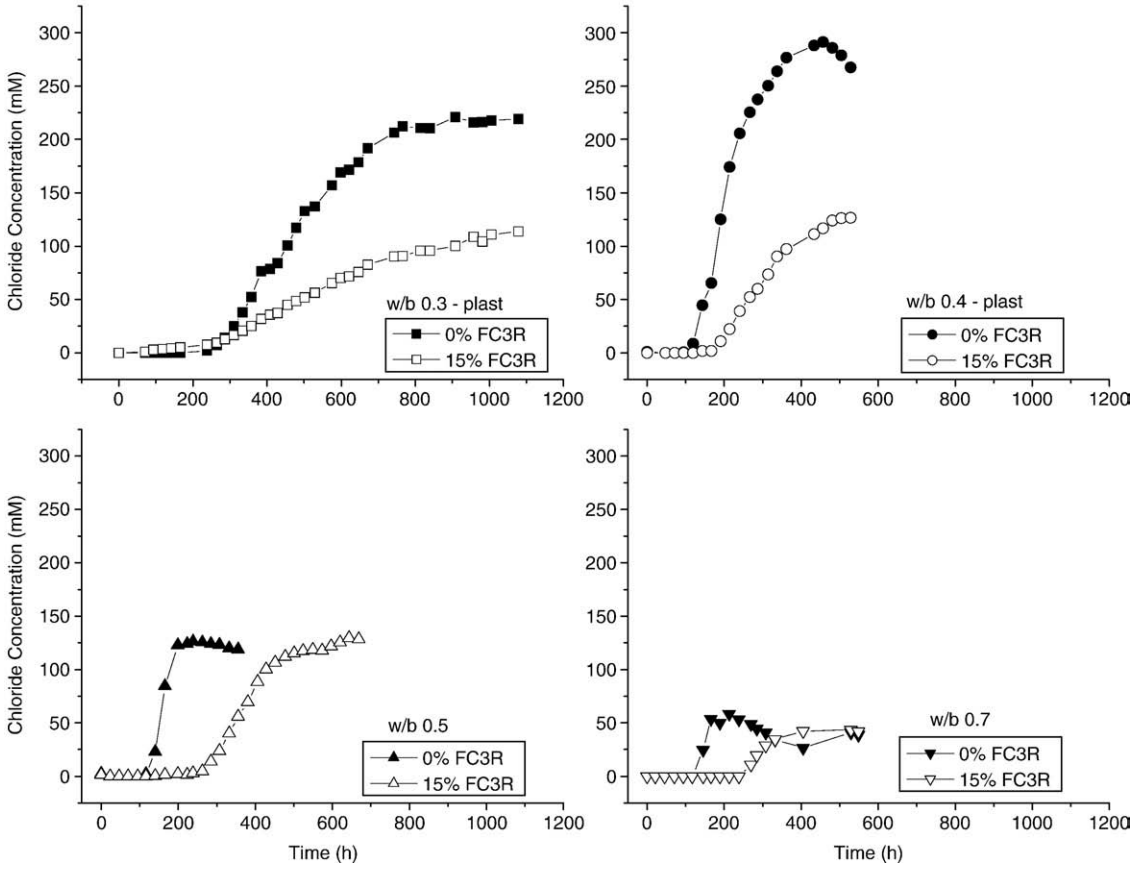

Fig. 10. Evolution of chloride concentration in the migration tests for all the w/b ratios.

Table 5
Parameters obtained from the migration tests for mortars with different w/b ratios and different levels of FC3R substitution

w/b ratio	FC3R (%)	Slope (mM/h)	Flux (μmol/(cm²h))	Time lag, τ (h)	Voltage (V)	D_{ns} (10^{-12} m²/s)	D_s (10^{-12} m²/s)
0.3 (plast)	0	0.551	8.21	240.7	7.94	1.67	1.67
	5	0.392	5.81	270.5	8.28	1.24	1.05
	10	0.232	3.45	355.2	7.90	1.09	0.69
	15	0.183	2.76	327.7	7.81	1.07	0.56
	20	0.195	2.95	380.7	7.80	1.03	0.59
0.4 (plast)	0	1.615	23.34	140.1	7.33	2.12	4.94
	5	1.219	18.11	145.3	7.60	1.70	3.30
	10	0.834	12.54	162.4	7.34	1.50	2.65
	15	0.600	8.49	162.7	7.33	1.45	1.84
	20	0.536	8.01	172.5	8.02	1.49	1.54
0.5	0	1.772	22.71	156.7	7.11	2.92	5.27
	5	0.866	11.61	257.7	7.72	2.64	2.52
	10	0.882	11.57	268.0	7.73	2.48	2.40
	15	0.618	7.68	255.5	8.22	2.32	1.58
	20	0.538	6.89	277.2	8.20	2.10	1.40
0.7	0	0.988	12.71	120.6	6.18	4.31	5.35
	5	0.866	11.09	147.4	5.67	4.19	3.21
	10	0.578	7.03	226.8	6.11	3.52	1.95
	15	0.474	6.15	225.1	5.98	2.70	1.81
	20	0.437	5.53	239.4	5.99	2.54	1.60

both parameters when the quantity of FC3R is increased. It can be appreciated in Fig. 13 that a 15% of cement substitution by FC3R for a mortar with w/b ratio of 0.7 provides a similar value for D_{ns} to that obtained with a mortar without FC3R and w/b ratio of 0.5. The effect of decreasing the w/b ratio of mortars also produces reductions of the diffusion coefficients, although this effect is more clearly seen for D_{ns} in Fig. 13.

3.3. Mercury intrusion porosimetry analyses

In order to assess the effect of FC3R on the porosity of mortars, mercury intrusion porosimetry analyses were performed on some selected mortars (w/b ratio of 0.5, and 0 and 15% of FC3R). Fig. 15 shows the pore size distribution of the mortars analysed. It can be observed that the incorporation of FC3R produces a reduction of the pore diameters, specially in the pore diameter range below 0.5 μm.

Fig. 16 presents the capillary and gel porosities of mortars analysed by mercury intrusion porosimetry. In this work, gel porosity has been considered as the pore volume with diameter under 0.05 μm, and capillary porosity has been considered as the pore volume within the pore range of 0.05–3 μm. It can be observed that mortars with 15% of FC3R present an important reduction of capillary porosity. Additionally, the migration process, in general, slightly increases capillary porosity. This effect can be explained taking into account that electrochemical anodic reactions generate H^+, thus decreasing the pH of the anolyte. This increasingly acid electrolyte can interact with the mortar surface, and this reaction has been shown to increase the porosity of the anodic side of the mortar sample during the migration experiment [28,29]. Mortars with 15% of FC3R present a higher proportion of gel pores, but this pore range does not contribute significantly to diffusion processes due to its very low size [29–31].

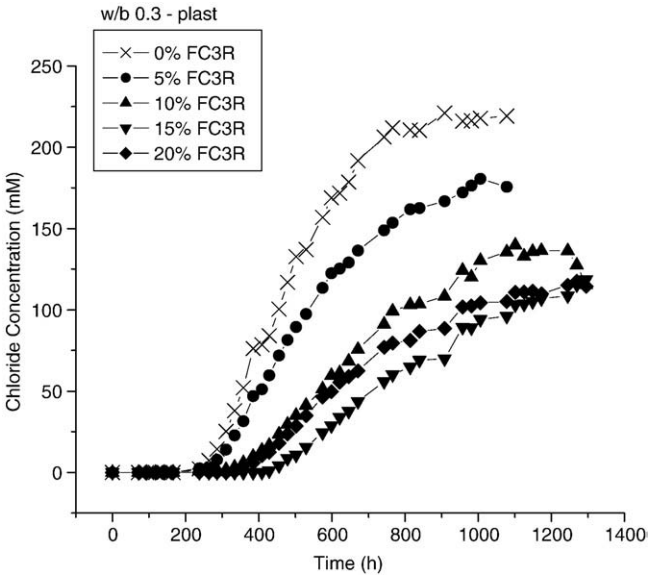

Fig. 12. Evolution of the chloride concentration in the anodic chamber for mortars with increasing level of cement substitution and w/b of 0.3.

3.4. Mortar resistivity measurements

Additionally, it was studied the electrical resistivity of mortars. The cementitious matrix of mortars can be considered as an electrical insulator. When a voltage is applied to a mortar specimen, the charge transport takes place by the movement of ions in the pore solution. In

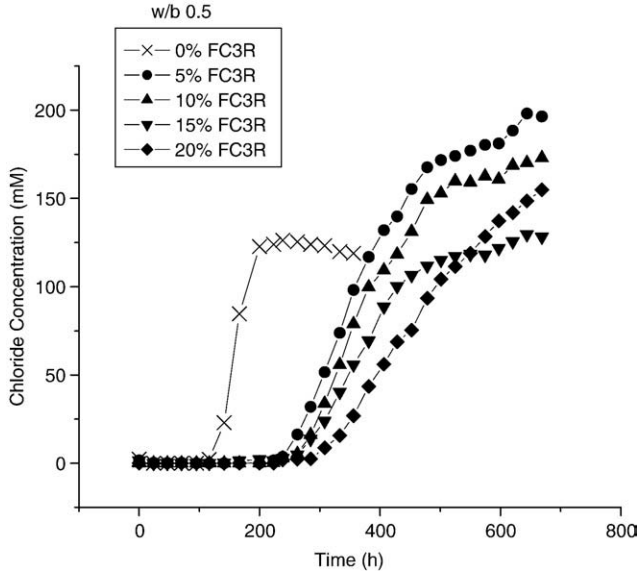

Fig. 11. Evolution of the chloride concentration in the anodic chamber for mortars with increasing level of cement substitution and w/b of 0.5.

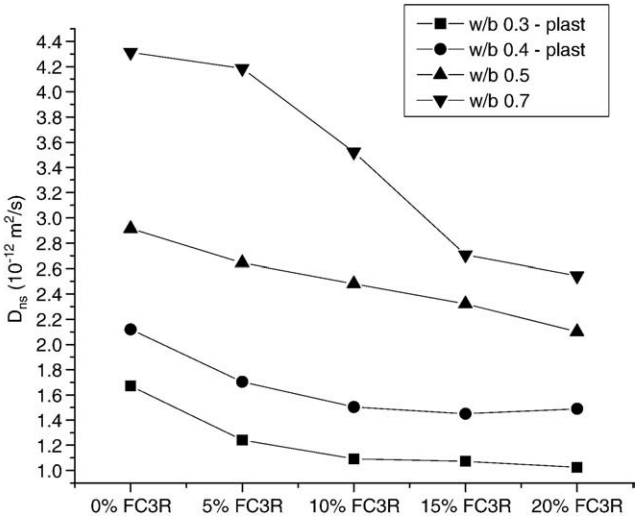

Fig. 13. Non-steady-state chloride diffusion coefficient of OPC/FC3R mortars.

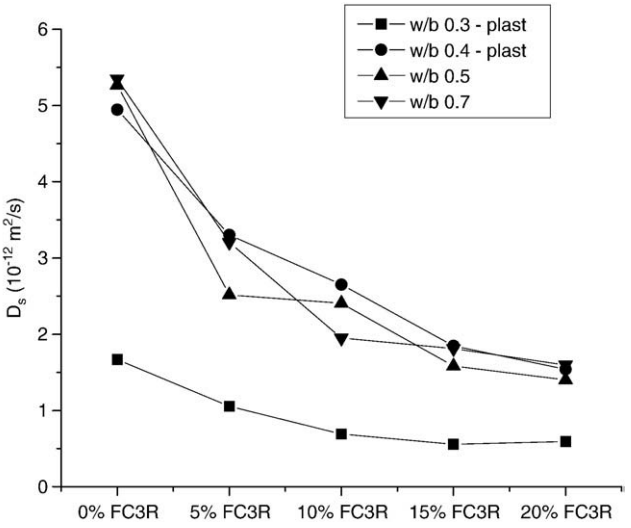

Fig. 14. Steady-state chloride diffusion coefficient for OPC/FC3R mortars.

this case, migration tests are also affected by the resistivity of mortars, since chloride ions are charge carriers under an applied voltage. For this reason, once the chloride binding capacity of the mortar has been exhausted, the diffusion of chlorides is indirectly determined by the resistivity (ρ) of the mortar and, therefore, resistivity measurements are related to steady-state chloride diffusion coefficients [14].

Fig. 17 shows the resistivity obtained for all the mortars studied. It can be observed that, when the cement substitution by FC3R is increased, an increase in the resistivity of the mortar takes place. Additionally, mortars with w/b ratio of 0.4, 0.5 and 0.7 present very similar resistivity values, while mortar with w/b ratio of 0.3 offers a significant increase in this parameter respect to the other ones. The trends observed for this parameter are very similar but opposite to those presented by steady-state diffusion coefficients, see Fig. 14. Fig. 18 shows a linear relationship between D_s and the inverse of resistivity. The best fit of the points of Fig. 17 is represented by Eq. (8).

$$D_s = 20.03 \cdot \frac{1}{\rho} - 0.29 \tag{8}$$

where D_s is expressed in $\times 10^{-12}$ m^2/s, and ρ in kΩ cm. This fitting has a correlation coefficient, R^2, of 0.948.

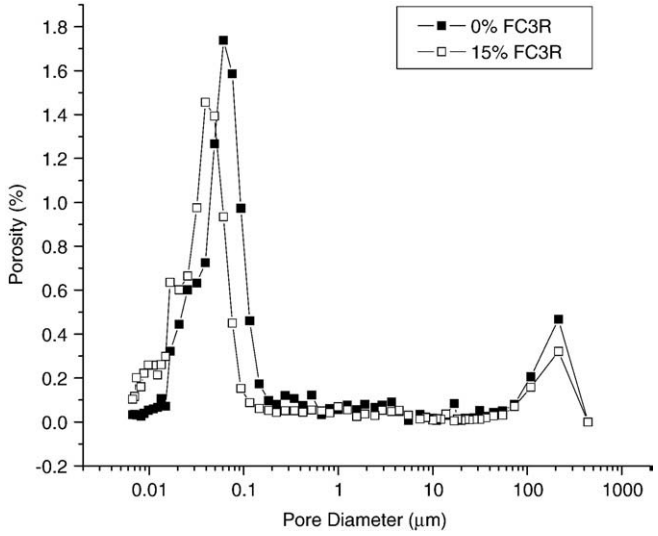

Fig. 15. Mercury intrusion porosimetry of mortars with 15% of FC3R and without FC3R, before migration tests (w/b ratio of 0.5).

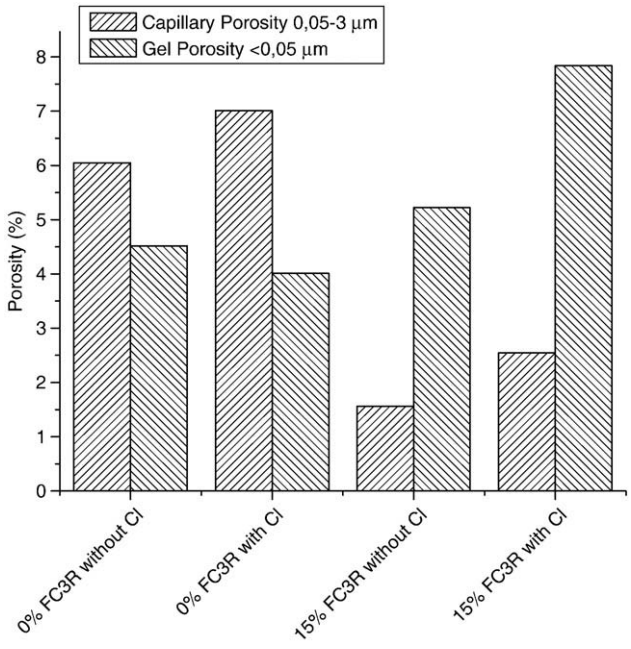

Fig. 16. Capillary and gel porosity of mortar with 15% and without FC3R, before and after the migration test. w/b ratio of 0.5.

The almost inverse relationship between chloride diffusion coefficient and resistivity found in Eq. (8) may be considered a proof of the applicability of the Nernst–Einstein relation for the mortars containing FC3R studied in this work. This relation was shown before to be applicable to water saturated concrete [14] and to partially saturated concrete [32].

3.5. Influence of the FC3R content on the corrosion rate

Fig. 19 shows the evolution of Icorr and Ecorr of steels embedded in mortars with different levels of cement substitution by FC3R. In this figure, the results corresponding to the first three stages are presented. In this graph, a boundary region between 0.1 and 0.2 μA/cm^2 separates the inactive corrosion rate zone and the active corrosion rate zone [33]. The aim of the first stage, in which specimens were stored at 100% of relative humidity, was to develop properly the cementitious matrix before they were subjected to more aggressive

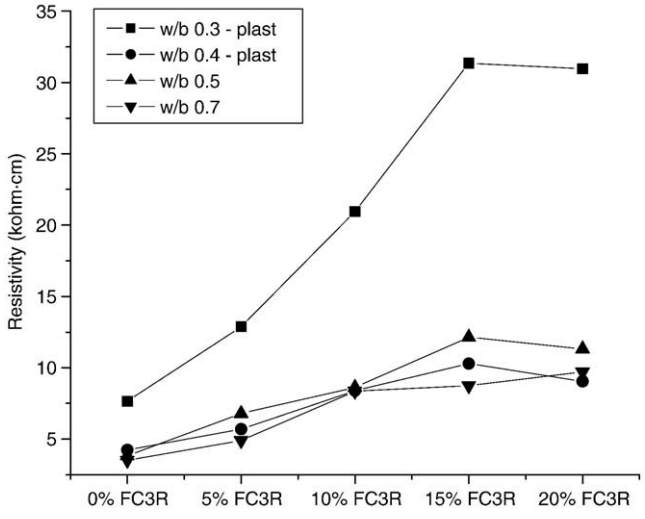

Fig. 17. Resistivity of mortars with different w/b ratios and cement substitution by FC3R.

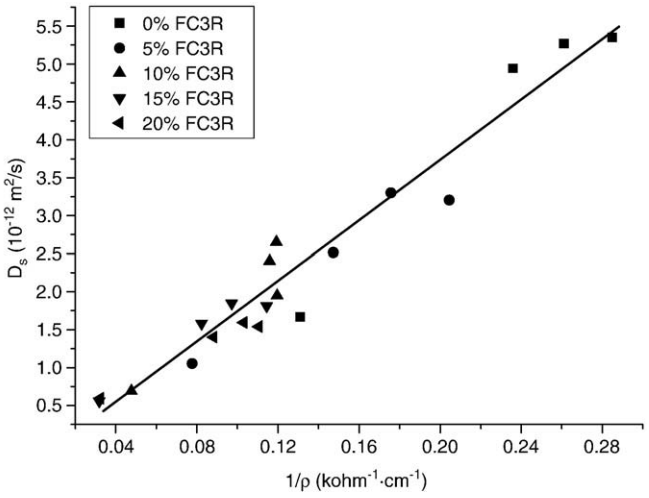

Fig. 18. Relationship between steady-state chloride diffusion coefficient and the inverse of resistivity of mortars.

storing conditions. At the beginning, steel electrodes show high corrosion rates because the passivation process takes some time to produce the passive layer in the steel surface [34,35]. Then, Icorr values progressively decrease towards the inactive corrosion zone indicating that steels are passivated. In a similar way, Ecorr values are initially low and after some time they increase to more passive potentials.

After the first stage, specimens were partially submerged in a NaCl 0.5 M solution. After the immersion, a decrease in corrosion potential can be observed due both to different condition of oxygen availability when the specimen is moved from a 100% RH environment to a submerged situation, and to the penetration of chlorides through the mortar cover and the consequent increase in the chloride concentration at the steel surface. Steels embedded in mortars with 10% FC3R showed the highest potential. Those ones embedded in mortars with 0% of FC3R offered intermediate values of corrosion potential. Finally, steels embedded in mortar with 20% of FC3R presented the lowest corrosion potential values. These differences in the Ecorr value are not reflected in increments in the corrosion rate of steels, except for steels embedded in mortar with 20% of FC3R. A beneficial effect of the presence of FC3R can be observed, but care must be taken in not surpassing the 15% of replacement. The higher corrosion rate values offered by steels embedded in mortar with 20% of FC3R are probably due to the loss on workability that appears when using FC3R in high proportions [2]. The compaction of mortars with such a high quantity of FC3R is more difficult and porosity of this mortar is probably increased respect to the other ones. For this reason the concentration of chlorides that can reach the steel surface is higher for this mortar, and the corrosion rate increases consequently. Figs. 19 and 20 show that for mortars with lower cement replacement (up to 15%) the presence of FC3R produces an increase in the corrosion potential as a result of the more compact structure of the cementing paste and an improved chloride binding capacity. The first factor is produced by the formation of additional cementing products, which are produced in the pozzolanic reaction. The second one occurs because the higher Al_2O_3 content in FC3R enhances the chloride binding capacity of the mortar, and as a consequence, the concentration of free chlorides at the steel surface is reduced. Additionally, it is clear that any addition of FC3R up to 15% produces lower corrosion rates than that observed in steels embedded in mortar without FC3R.

In the third stage, mortars were stored again in an ambient of 100% of relative humidity to observe the evolution of the corrosion after the chloride attack. Icorr and Ecorr do not show appreciable changes, except steels embedded in mortar with 20% of FC3R, whose corrosion potential increases and corrosion rate decreases. This later phenomenon maybe is based on variations in the degree of water saturation of this mortar.

3.6. Influence of the w/b ratio on the corrosion rate

Fig. 20 shows the evolution of corrosion rate and corrosion potential of steels embedded in mortars with w/b of 0.5 and 0.7 and cement substitution by FC3R of 0% and 15%, while they were subjected to the same stages than those previously commented. In general, similar trends to those above mentioned are appreciated.

As it would be expected, steels embedded in mortars with higher w/b ratio offered higher corrosion rates. In the stage in which specimens were partially submerged in NaCl 0.5 M solution, little

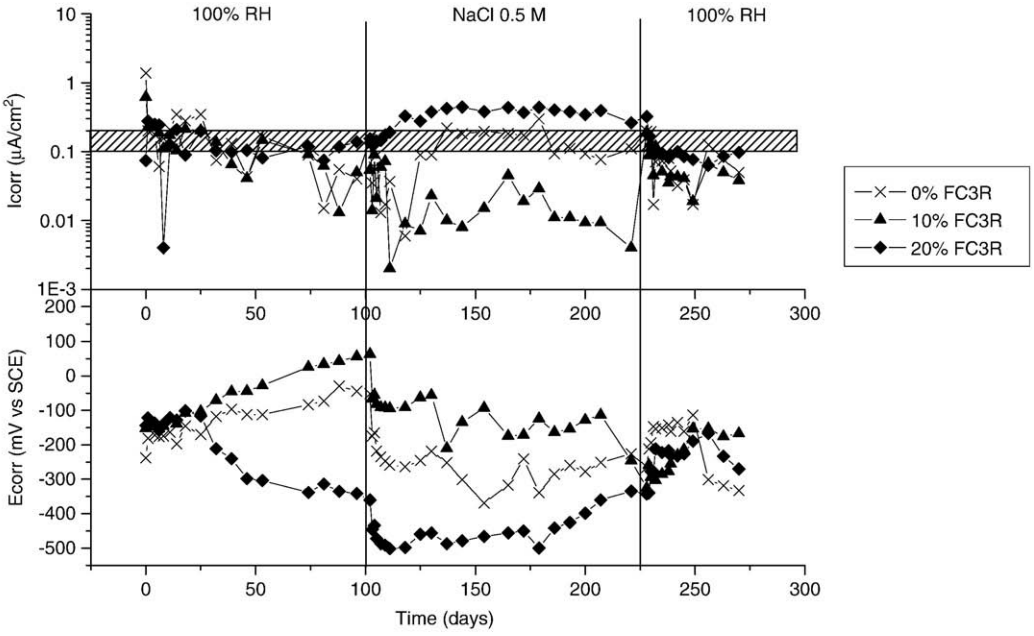

Fig. 19. Corrosion rate and corrosion potential of steels embedded in cement-FC3R mortar specimens with w/b of 0.5.

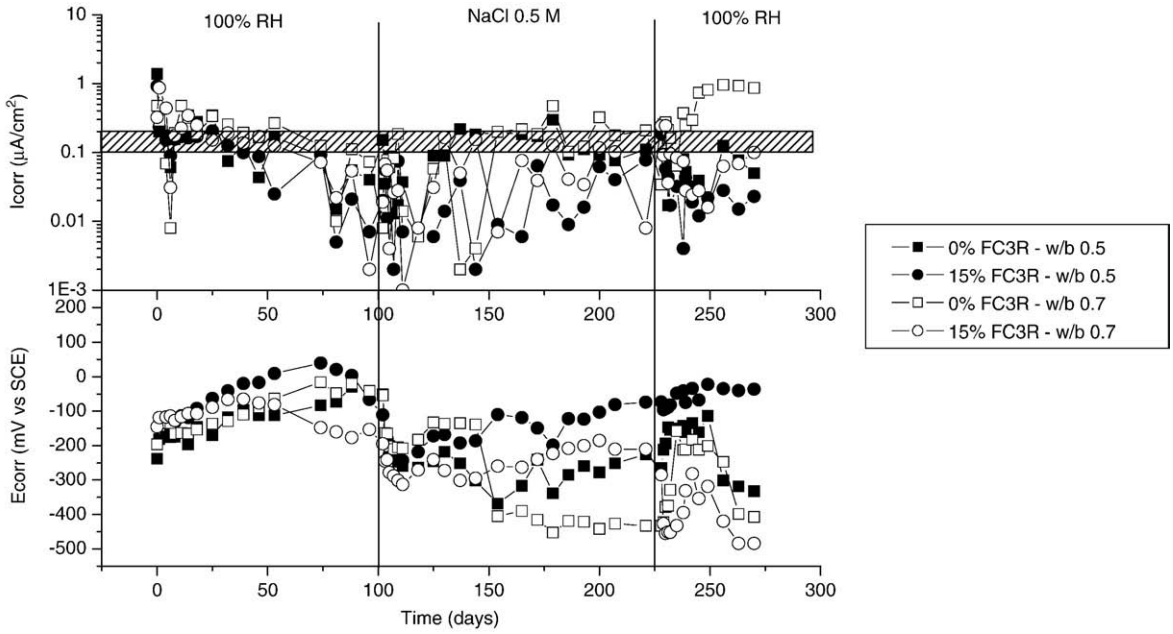

Fig. 20. Corrosion rate and corrosion potential of steels embedded in cement-FC3R mortar specimens with w/b of 0.5 and 0.7.

differences are observed in the corrosion rate values, although, in general, steels embedded in mortars with 15% of FC3R show lower corrosion rate values than those embedded in mortars without FC3R. These differences are more noticeable in the Ecorr part of the graph. Steels embedded in mortars with 15% of FC3R present higher corrosion potentials than steels of mortars with 0% of FC3R, and steels embedded in mortars with w/b of 0.5 also show higher corrosion potential than that observed in steels of mortars with w/b of 0.7.

In Table 6, mean Ecorr values of steels during the immersion in NaCl 0.5 M solution are presented, confirming the observations previously noted. When the w/b ratio is increased, a higher concentration of both oxygen and chlorides are expected at the steel surface, so the risk of corrosion is increased. The effect of cement replacement by FC3R is again a reduction in the porosity and an increase in the chloride binding capacity, which can be observed for both w/b ratios, 0.5 and 0.7. It is significant that the presence of 15% of FC3R in the mortar with a w/b of 0.7 produces that steels embedded in it present a higher corrosion potential than those embedded in mortar without FC3R and w/b of 0.5. This fact clearly shows the level of improvement that the addition of FC3R to mortar formulations can offer to prevent chloride-induced corrosion of steels.

In the third stage of Fig. 20, in which specimens were stored in an environment of 100% of relative humidity, a sharp increase in the corrosion rate of steels embedded in mortar with w/b of 0.7 and 0% of FC3R is observed. This increase is produced by the fact that chlorides reached the steel surface of this mortar at sufficient concentration to provoke the depassivation of the steel. Since specimens are not immersed in this stage the oxygen diffusion through the mortar cover is higher and as a result, if the steel was depassivated by the action of chlorides, the corrosion rate increases. This phenomenon was only observed in this mortar because its chloride ingress resistance is the lowest, since it has high porosity and poor chloride binding capacity.

Table 6
Corrosion potentials of steels embedded in mortars submerged in NaCl 0.5 M solution

w/b ratio	Mean Ecorr (mV vs SCE)	
	0% FC3R	15% FC3R
0.5	−283	−115
0.7	−424	−228

3.7. Influence of carbonation after the chloride attack on the corrosion rate

After the stages in which specimens were subjected to the action of chlorides, they were stored in a carbonation chamber. Carbonation can seriously damage reinforced concrete because this process reduces the pH of the pore solution and, consequently, steels lose their passive state. When the concrete cover is contaminated by chlorides, some of them are bound to the cementitious matrix to form Friedel's salt. When chloride-contaminated concrete is carbonated, additional risk apart from carbonation is produced, since those chlorides bound can be released to the pore solution as a consequence of the reduction of the pH. If the pH of the pore solution drops, Friedel's salt decomposes as shown in Eq. (7) [25–27].

Fig. 21 presents the evolution of Icorr and Ecorr of steels embedded in mortars with different level cement substitution by FC3R and a w/b ratio of 0.5 during the carbonation process that specimens experienced after the chloride attack. In this graph, it can be observed that carbonation produced an increase in Icorr values for all steel electrodes, although it was higher for those embedded in mortar without FC3R. Additionally, this increase in Icorr values was accompanied by the consequent decrease in Ecorr due to the depassivation of steel surface, although no significant differences are observed between different electrodes.

In the final stage, in which specimens were stored in an ambient of 80% of relative humidity to observe the evolution of corrosion parameters with a higher oxygen concentration (inside the carbonation chamber, oxygen concentration is very low), an additional increase of Icorr values and decrease of Ecorr values were registered. The highest Icorr values were presented for steels embedded in mortars without FC3R, thus even after the release of chlorides bound as Friedel's salt, the behaviour offered by FC3R mortars is better, probably due to the more compact structure of substituted mortars.

Fig. 22 shows the evolution of Icorr and Ecorr of steels embedded in mortars with different level cement substitution by FC3R and a w/b ratio of 0.7 during the carbonation process that specimens experienced after the chloride attack. The same changes previously commented for Fig. 21 are observed for steels embedded in mortars with w/b ratio of

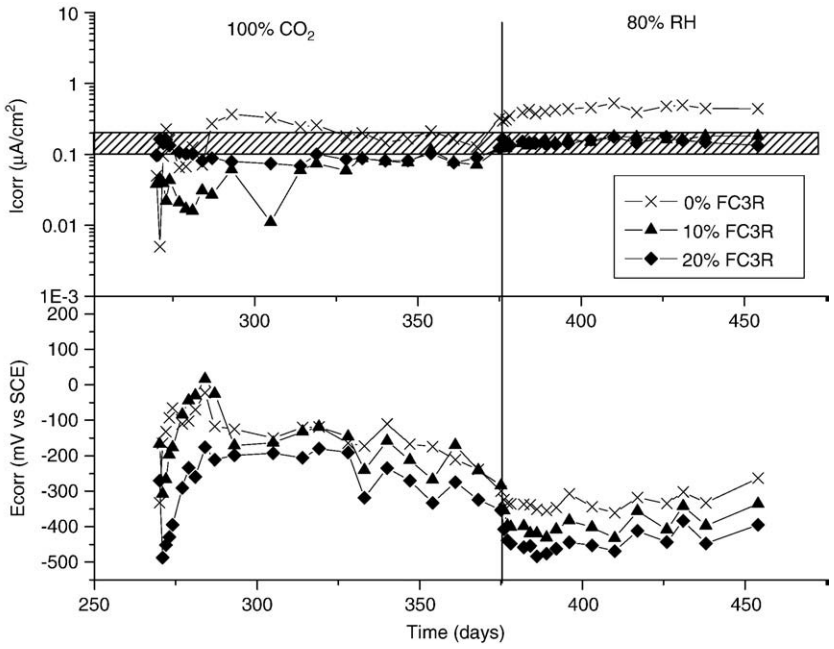

Fig. 21. Corrosion rate and corrosion potential of steels embedded in cement-FC3R mortar specimens with w/b of 0.5. Carbonation after the chloride attack.

0.7. However, the increase of Icorr and the decrease of Ecorr are higher due to the higher porosity of these mortars. Again, in the carbonation stage, although all Icorr values are very high, corrosion rate decreases when the cement substitution by FC3R is increased. In the final stage, at the end of the experiment, steels embedded in mortars without FC3R still presented the highest Icorr values, so it should be noted then, that the presence of FC3R after such aggressive storing conditions is positive for the corrosion behaviour of steels.

3.8. Study of the chlorides depassivation threshold

Fig. 23 presents the evolution of Icorr and Ecorr of steels embedded in mortars without FC3R, which were contaminated by the incorporation of different quantities of chlorides in the mixing water. At the beginning of the measurements, high Icorr values are observed because the formation of the passive layer at the steel surface needs some time to be properly developed. As expected, the corrosion rate increases when the amount of chlorides included in the mortar is increased from 0% to 5% by cement mass. Nevertheless, steels embedded in mortars with up to 1% of chlorides does not present active corrosion rate values, while those embedded in mortars with 2% and 5% of chlorides show high corrosion rates in the active corrosion zone. For this reason, it could be stated that the chloride threshold for mortars with plain Portland cement is situated between 1% and 2% of chloride content by cement mass. Consequently to the Icorr values registered, Ecorr values are also ordered in an opposite way. The higher

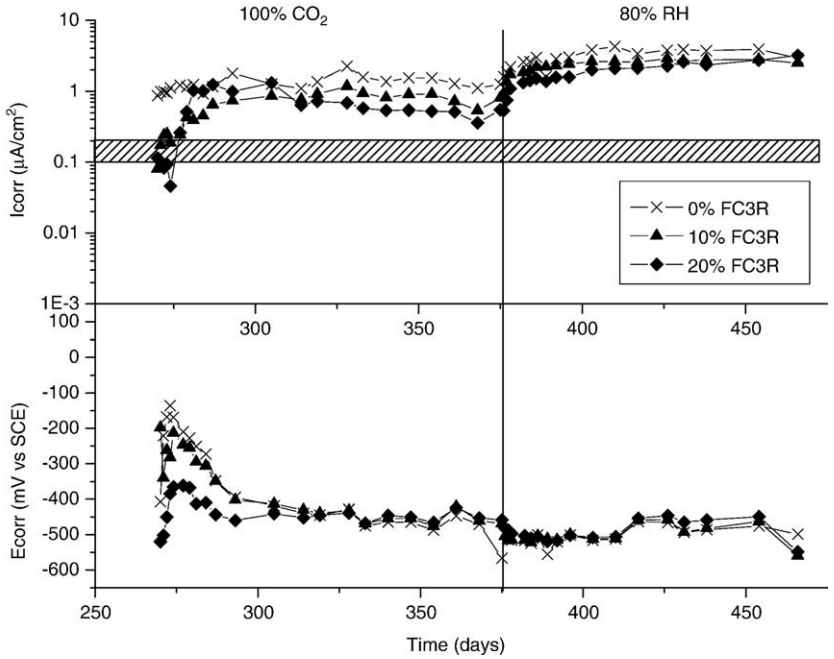

Fig. 22. Corrosion rate and corrosion potential of steels embedded in cement-FC3R mortar specimens with w/b of 0.7. Carbonation after the chloride attack.

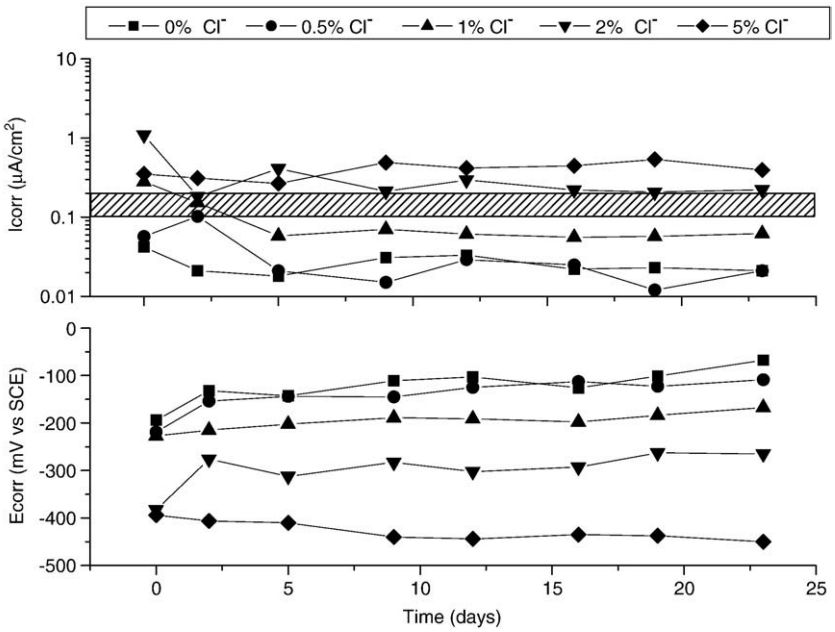

Fig. 23. Evolution of corrosion rate and corrosion potential of steels embedded in cement mortars without FC3R and different level of chloride included in mixing water. w/b ratio of 0.5.

is the quantity of chlorides, the lower is the Ecorr. It should be noted the no differences are appreciable between Ecorr values of steels embedded in mortars with 0% of chlorides and 0.5% of chlorides. This suggests that approximately 0.5% of chlorides are bound in the cementitious matrix as Friedel's salt.

Fig. 24 shows the evolution of Icorr and Ecorr of steels embedded in mortars with 15% of cement replacement by FC3R, which were contaminated by the incorporation of different quantities of chlorides in the mixing water. In this graph it can be noted again that when the amount of chlorides is increased, the Icorr increases and the Ecorr decreases.

Steels embedded in mortars with 15% of FC3R and such a high amount of chlorides of 2% present stable Icorr values in the inactive corrosion zone, so the chlorides threshold for mortars incorporating 15% of FC3R is situated in a quantity above 2%, which implies a significant improvement in protection that this binder offers to steels.

Regarding the Ecorr values observed for steels embedded in mortars with 15% of FC3R, it can be noted that there are no differences for steels of mortars with 0%, 0.5% and 1% of chloride. As it was previously commented, this fact would suggest that the amount of free chlorides is almost the same for these mortars, i.e. that 1% of chlorides are bound in the cementitious matrix as Friedel's salt. This

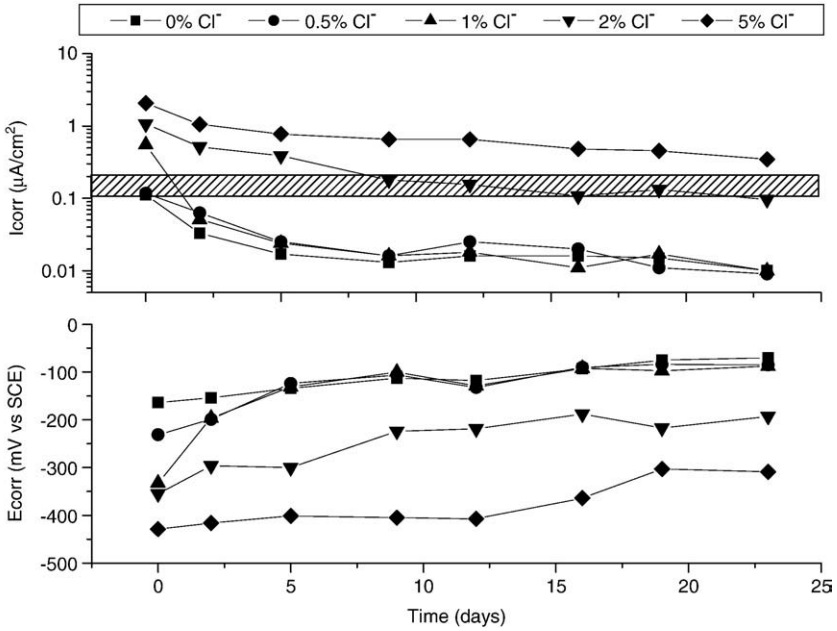

Fig. 24. Evolution of corrosion rate and corrosion potential of steels embedded in cement mortars with 15% of FC3R and different level of chloride included in mixing water. w/b ratio of 0.5.

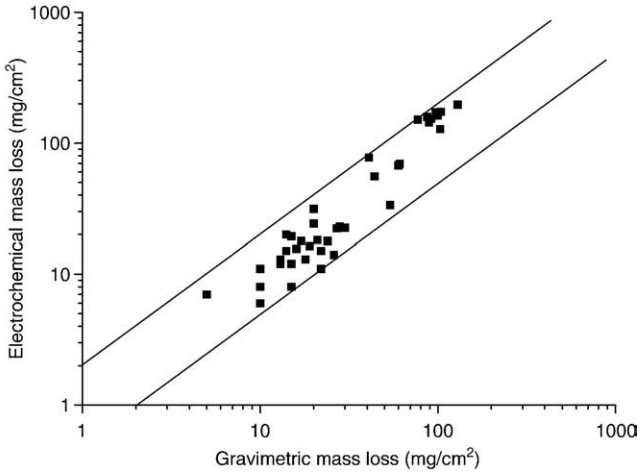

Fig. 25. Comparison between electrochemical mass loss and gravimetric mass loss.

represents a significant improvement in the chloride binding capacity of mortars with FC3R respect to mortars without FC3R.

3.9. Checking electrochemical measurements

Fig. 25 presents the comparison between electrochemical mass loss and gravimetric mass loss. It can be observed that all electrochemical measurements lay within the tolerance error area of the polarization resistance technique used for monitoring corrosion rates. This technique allows an error factor of 2 due to the error associated to *B* value in the Stern–Geary formula, which relates Icorr to polarization resistance (Rp) Eq. (9) [18]. For the steel–cement system *B* presents a value situated between 13 mV and 52 mV depending on the passive state of the steel. For this research a *B* value of 26 mV has been assumed.

$$\text{Icorr} = \frac{B}{\text{Rp}} \tag{9}$$

FC3R is a pozzolan that will influence both the porosity and the chloride binding capacity of cement mortars. Due to the formation of additional cementing products by the pozzolanic reaction, FC3R produces a more compact structure as it has been determined by mercury intrusion porosimetry. It has been observed that there is a shift of the porosity of the capillary pore range towards gel pore range.

Additionally, due to the high Al_2O_3 content of FC3R, the binding capacity of mortars that include FC3R in the mix, is increased significantly, as it has been observed in thermogravimetric tests. The higher formation of CAH and CASH phases offers a higher proportion of products capable to react with chlorides and bind them to the cementitious matrix.

These observations yield an improvement in the chloride ingress resistance that has been quantified in migration tests. On one hand, the time that chlorides need to penetrate the mortar is higher because the formation of Friedel's salt together with the more reduced porosity, delays the advance of the chlorides front. When the chlorides get through the mortar the net flux of chlorides is reduced because, again, the reduced porosity hinders the penetration of chlorides.

In other works, FC3R has shown very high pozzolanic activity, enhancing in a large extent mechanical properties of mortars or concretes. This fact, together with the results presented in this research, produces a very competitive binder for steel reinforced concrete production in environments where high concentration of chlorides are going to be present.

4. Conclusions

In this research, the chloride ingress resistance of mortars incorporating FC3R as cement replacement has been studied. The incorporation of increasing amounts of FC3R as cement replacement in quantities up to 20% produces higher formation of CAH and CASH phases. This fact enhances the chloride binding capacity of binders. Additionally, the pozzolanic reaction of FC3R reduces the capillary porosity of cementitious matrices. Both phenomena reduce the non-steady-state and steady-state chloride diffusion coefficient of mortars. An inverse relationship between electrical resistivity and steady-state diffusion coefficient has been found for the tested mortars.

The improvement in the chloride ingress resistance led to an increase of the resistance to steel corrosion for the FC3R containing mortars. It has been found that the chlorides threshold is higher than 2% by cement mass for mortars incorporating 15% of FC3R as cement replacement, offering lower corrosion rates for steels at a given chloride concentration added to the mix. Therefore, FC3R is highly recommended for its use in reinforced concrete structures exposed to chloride-contaminated environments.

Acknowledgements

E. Zornoza thanks the Ministerio de Educación y Ciencia from Spain for his doctorate grant (Program FPU, Ref. 20023421). This work has been financially supported by the Ministerio de Ciencia y Tecnología of Spain through project MAT 2001-2694, and by the Ministerio de Educación y Ciencia of Spain and Fondo Europeo de Desarrollo Regional (FEDER) through project BIA2006-05961.

References

[1] A. Neville, Chloride attack of reinforced concrete: an overview, Materials and Structures 28 (1995) 63–70.
[2] J. Payá, J. Monzó, M.V. Borrachero, Fluid catalytic cracking catalyst residue (FC3R): an excellent mineral by-product for improving early-strength development of cement mixtures, Cement and Concrete Research 29 (1999) 1773–1779.
[3] K.-C. Hsu, Y.-S. Tseng, F.-F. Ku, N. Su, Oil cracking waste catalyst as an active pozzolanic material for superplasticized mortars, Cement and Concrete Research 31 (2001) 1815–1820.
[4] Pacewska, M. Bukowska, I. Wilinska, M. Swat, Modification of the properties of concrete by a new pozzolan: a waste catalyst from the catalytic process in a fluidized bed, Cement and Concrete Research 32 (2002) 145–152.
[5] Pacewska, I. Wilinska, M. Bukowska, W. Nocun-Wczelik, Effect of waste aluminosilicate material on cement hydration and properties of cement mortars, Cement and Concrete Research 32 (2002) 1823–1830.
[6] J. Payá, J. Monzó, M.V. Borrachero, F. Amahjour, I. Girbés, S. Velázquez, L.M. Ordónez, Advantages in the use of fly ashes in cements containing pozzolanic combustion residues: silica fume, sewage sludge ash, spent fluidized bed catalyst and rice husk ash, Journal of Chemical Technology and Biotechnology 77 (2002) 331–335.
[7] J. Payá, J. Monzó, M.V. Borrachero, S. Velázquez, Evaluation of the pozzolanic activity of fluid catalytic cracking residue (FCC): thermogravimetric analysis studies on FCC-Portland cement pastes, Cement and Concrete Research 33 (2003) 603–609.
[8] J.-H. Wu, W.-L. Wu, K.-C. Hsu, The effect of waste oil-cracking catalyst on the compressive strength of cement pastes and mortars, Cement and Concrete Research 33 (2003) 245–253.
[9] W.-L. Wu, J.-H. Wu, K.-C. Hsu, D.-S. Yen, Subproducto del fraccionamiento catalítico del petróleo: características, actividad puzolánica y su efecto en las propiedades del mortero, Cemento Hormigón 850 (2003) 18–25.
[10] H.-L. Chen, Y.-S. Tseng, K.-C. Hsu, Spent FCC catalyst as a pozzolanic material for high-performance mortars, Cement and Concrete Composites 26 (2004) 657–664.
[11] J. Payá, J. Monzó, M.V. Borrachero, S. Velázquez, M. Bonilla, Determination of the pozzolanic activity of fluid catalytic cracking residue. Thermogravimetric analysis studies on FC3R-lime pastes, Cement and Concrete Research 33 (2003) 1085–1091.
[12] E. Peris-Mora, J. Payá, J. Monzó, Influence of different sized fractions of a fly ash on workability of mortars, Cement and Concrete Research 23 (1993) 917–924.
[13] American Standard ASTM C 1202-91, Standard test method for electrical indication of concrete's ability to resist chloride ion penetration, American Society for Testing Materials (1991).
[14] C. Andrade, Calculation of chloride diffusion coefficients in concrete from ionic migration measurements, Cement and Concrete Research 23 (1993) 724–742.
[15] M. Castellote, C. Andrade, C. Alonso, Measurements of the steady and non-steady-state chloride diffusion coefficients in a migration test by means of monitoring the conductivity in the anolyte chamber. Comparison with natural diffusion tests, Cement and Concrete Research 31 (2001) 1411–1420.
[16] L.C. Lange, C.D. Hills, A.B. Poole, The influence of mix parameters and binder choice on the carbonation of cement solidified wastes, Waste Management 16 (1996) 749–756.
[17] Y. Lo, H.M. Lee, Curing effects on carbonation of concrete using a phenolphthalein indicator and Fourier-transform infrared spectroscopy, Building and Environment 37 (2002) 507–514.

[18] M. Stern, A.L. Geary, A theoretical analysis of the shape of polarization curves, Journal of Electrochemical Society 104 (1957) 56–63.
[19] G. Villain, G. Platert, Two experimental methods to determine carbonation profiles in concrete, ACI Materials Journal 103 (2006) 265–271.
[20] V.S. Ramachandran (Ed.), Application of Differential Thermal Analysis in Cement Chemistry, Chemical Publishing Company, Inc., New York, 1969.
[21] N. Saikia, S. Kato, T. Kojima, Thermogravimetric investigation on the chloride binding behaviour of MK-lime paste, Thermochimica Acta 444 (2006) 16–25.
[22] A.K. Suryavanshi, J.D. Scantlebury, S.B. Lyon, Mechanism of Friedel's salt formation in cements rich in tricalcium aluminate, Cement and Concrete Research 26 (1996) 717–727.
[23] M.R. Jones, D.E. Macphee, J.A. Chudek, G. Hunter, R. Lannegrand, R. Talero, S.N. Scrimgeour, Studies using ^{27}Al MAS NMR of AF_m and AF_t and the formation of Friedel's salt, Cement and Concrete Research 33 (2003) 177–182.
[24] U.A. Birnin-Yauri, F.P. Glasser, Friedel's salt, $Ca_2Al(OH)_6(Cl,OH)\cdot 2H_2O$: its solid solutions and their role in chloride binding, Cement and Concrete Research 28 (1998) 1713–1723.
[25] S. Goñi, A. Guerrero, Accelerated carbonation of Friedel's salt in calcium aluminate paste, Cement and Concrete Research 33 (2003) 21–26.
[26] A.K. Suryavanshi, R.N. Swamy, Stability of Friedel's salt in carbonated concrete structural elements, Cement and Concrete Research 26 (1996) 729–741.
[27] L. Jiang, B. Lin, Y. Cai, A model for predicting carbonation of high-volume fly ash concrete, Cement and Concrete Research 30 (2000) 699–702.
[28] I. Sánchez, X.R. Nóvoa, G. de Vera, M.A. Climent, Microstructural modifications in Portland cement concrete due to forced ionic migration tests, Study by impedance spectroscopy, Cement and Concrete Research 38 (7) (2008) 1015–1025.
[29] M. Castellote, C. Andrade, C. Alonso, Changes in concrete pore size distribution due to electrochemical chloride migration trials, ACI Materials Journal 96 (3) (1999) 314–319.
[30] R.A. Cook, K.C. Hover, Mercury intrusion porosimetry of hardened cement pastes, Cement and Concrete Research 29 (1999) 933–943.
[31] C.C. Yang, L.C. Wang, The diffusion characteristic of concrete with mineral admixtures between salt ponding test and accelerated chloride migration test, Materials Chemistry and Physics 85 (2004) 266–272.
[32] M.A. Climent, G. de Vera, J.F. López, E. Viqueira, C. Andrade, A test method for measuring chloride diffusion coefficients through nonsaturated concrete. Part I: the instantaneous plane source diffusion case, Cement and Concrete Research 32 (2002) 1113–1123.
[33] C. Andrade, J.A. González, Quantitative measurements of corrosion rate of reinforcing steels embedded in concrete using polarization resistance measurements, Werkstoffe und Korrosion 29 (1978) 515–523.
[34] P. Garcés, E.G. Alcocel, J.J. Martínez Pérez, J. Payá, L.G. Andión, Effect of sewage sludge ash (SSA) on the mechanical performance and corrosion levels of reinforced Portland cement mortars, Materiales de Construcción 56 (2006) 31–43.
[35] A. Poursaee, C.M. Hansson, Reinforcing steel passivation in mortar and pore solution, Cement and Concrete Research 37 (2007) 1127–1133.